

MambaRecon: MRI Reconstruction with Structured State Space Models

Yilmaz Korkmaz, Vishal M. Patel

Department of Electrical and Computer Engineering, Johns Hopkins University

{ykorkma1,vpatel36}@jhu.edu

Abstract

Magnetic Resonance Imaging (MRI) is one of the most important medical imaging modalities as it provides superior resolution of soft tissues, albeit with a notable limitation in scanning speed. The advent of deep learning has catalyzed the development of cutting-edge methods for the expedited reconstruction of MRI scans, utilizing convolutional neural networks and, more recently, vision transformers. Recently proposed structured state space models (e.g., Mamba) have gained some traction due to their efficiency and low computational requirements compared to transformer models. We propose an innovative MRI reconstruction framework that employs structured state space models at its core, aimed at amplifying both long-range contextual sensitivity and reconstruction efficacy. Comprehensive experiments on public brain MRI datasets show that our model sets new benchmarks beating state-of-the-art reconstruction baselines. Code will be available [here](#).

1 Introduction

Magnetic Resonance Imaging (MRI) is a highly prevalent imaging technique, favored for its superior soft tissue visualization capabilities. However, its use is limited by lengthy and expensive scanning process. As a result, there is a pressing need for accelerated MRI techniques to enhance its practical application in clinical settings. Sampling less k-space points (i.e., Fourier coefficients) below the Nyquist rate can expedite the scanning but it requires to solve an ill-posed reconstruction problem [28]. Compressed sensing (CS) solutions have been demonstrated to be powerful in reconstruction problems [32, 7, 29, 16]. However, despite their efficacy, CS methods suffer from their high sensitivity to hyper-parameters, which requires careful tuning to achieve optimal performance. Moreover, the iterative nature of most CS algorithms contributes to their computational inefficiency, making them inherently slow compared to

other approaches.

Following the emergence of deep learning, iterative approaches have been increasingly supplanted by deep learning methods [42, 49, 6, 25]. These methods predominantly leverage convolutional neural networks (CNNs) which have proven to be highly effective in various image processing tasks with data-driven approaches. Along with the pure data-driven methods, various physics-guided reconstruction models have been proposed [46, 1, 38, 34]. In these models, the forward encoding operator, which includes the undersampling pattern and coil sensitivities in multi-coil setting, is also utilized in the model along with the under-sampled acquisitions to enhance the robustness and superior performance in the reconstruction [46]. However, CNNs are inherently constrained by their limited receptive fields, which restrict their ability to capture long-range dependencies and contextual information comprehensively [53].

In recent years, following the success of transformers in downstream computer vision tasks, transformer-based approaches have been introduced to address the limited receptive field of CNNs in the realm of MRI reconstruction [24, 15, 57, 19]. By incorporating transformer architectures, increased sensitivity to long-range dependencies and expanded effective receptive fields have been achieved. However, quadratic complexity of self-attention transformers with respect to input sequence length creates a computational burden [22, 24].

Structured state space models (SSMs) are one of the proposed solutions to address the quadratic complexity of self-attention transformers to efficiently model long sequences [12]. More recently, a new class of structured state space models (i.e., Mamba) has been proposed with input dependent parametrization and linearly scaled complexity with sequence length [11]. Mamba has shown a promising direction in large language models and recently been utilized in several vision tasks including classification [26], image segmentation [44, 31] and image restoration [14].

Inspired from these developments, in this paper we

propose a physics-guided MRI reconstruction framework utilizing structured state space models in its core with a very few number of trainable parameters. Our model benefits from the increased long-range contextual sensitivity along with the sub-quadratic complexity without omitting the underlying physical model by alternating between data-consistency and Mamba blocks. Comprehensive experiments demonstrate our model’s superior performance compared with the state-of-the-art MRI reconstruction models.

This paper makes the following contributions:

1. We propose a novel lightweight physics-guided MRI reconstruction model utilizing structured state space models as a core block. Our model enhances the long range sensitivity of the model by significantly increasing the effective receptive field.
2. We obtain superior performance in both complex multi-coil and magnitude single-coil public brain MRI datasets compared to the state-of-the-art reconstruction baselines.

2 Related Works

Data-Driven Convolution Based Models. Convolutional neural networks (CNNs) have been predominantly used in deep MRI reconstruction to learn the underlying mapping between under- and fully-sampled acquisitions. Wang et al. [42] proposed one of the first CNN-based framework for MRI reconstruction. Ye et al. [49] proposed a CNN-based model to efficiently solve general inverse problems. Lee et al. [25] offered a deep CNN-based model with residual connections for MRI reconstruction. Hyun et al. [21] utilized a reconstruction model employing a U-shaped network. Dar et al. [6] proposed a conditional generative adversarial network (GAN) following the success of GANs in image generation. Gungor et al. [13] proposed a test time adaptation approach with a diffusion-based model.

Physics-guided Convolution Based Models. Aggarwal et al. [1] proposed an unrolled model with a CNN backbone. Schlemper et al. [38] utilized a deep cascaded CNN to efficiently incorporate forward operator. Eo et al. [9] proposed a dual-domain physics-guided CNN-model. Yaman et al. [46] offered an innovative solution to eliminate supervision requirement via a self-supervised approach with an unrolled CNN backbone. Yang et al. [47] proposed an unified physics-guided model trained with alternating direction method of multipliers (ADMM) algorithm. Biswas et al. [3] proposed an extra smoothness regularization with a physics-guided network. Qin et al. [35] proposed a recurrent convolutional model for dynamic MRI reconstruction. Sri-ram et al. [39] proposed an unrolled variational model

utilizing both k-space and image domains. Yiasemis et al. [51] proposed a hybrid architecture performing optimization in k-space using an image domain refinement network.

Transformer-based Models. Following the success of transformer-based approaches in computer vision, Korkmaz et al. [24] proposed a zero-shot learned transformer model for unsupervised reconstruction. Guo et al. [15] offered a physics-guided model with a recurrent transformer backbone. Zhou et al. [56] proposed a dual-domain transformer model using both frequency and image domains. Huang et al. [19] adapted the computationally efficient Swin Transformer model for MRI reconstruction. Hu et al. proposed [18] a transformer based model with a special regularization to keep high frequency details. Fabian et al. [10] proposed an unrolled hybrid architecture employing transformers along with CNNs. Lyu et al. [30] offered a region-focused GAN with a transformer backbone. Zhao et al. [55] offered an adversarial model with a swin transformer backbone for MRI reconstruction.

Mamba in Medical Imaging. More recently, a couple of Mamba-based deep learning models have been utilized in various medical imaging tasks. Yue et al. [52] proposed a vision Mamba model for medical image classification. Xing et al. [45] offered a U-shaped mamba model for 3D image segmentation. Yang et al. [48] adapted Mamba for medical video object segmentation. Wang et al. [44] and Ruan et al. [37] proposed U-shaped Mamba-based models for medical image segmentation. Atli et al. [2] proposed a Mamba-based synthesis model for medical image translation.

Concurrently, Huang et al. [20] offered an arbitrarily masked Mamba-based model for medical image reconstruction and uncertainty estimation without taking physical model into account. Zou et al. [58] proposed a multi-domain Mamba-based reconstruction framework, however this work differs from our approach due to usage of fully-sampled auxiliary modality along with the target reconstruction. To best our knowledge, this is the first physics-guided SSM-based model for MRI reconstruction.

3 Background

3.1 Accelerated MRI Reconstruction

MRI reconstruction from partial k-space can be defined as follows

$$S_p C x = y_p, \quad (1)$$

where S_p is the partial Fourier operator, x is the target MR image, C is the coil sensitivity maps and y_p stands for the partially sampled k-space points. Reconstruction

of x from y_p leads to infinitely many solutions, thus solution requires regularization. Reconstruction objective with regularization can be formulated as

$$\hat{x} = \operatorname{argmin}_x \frac{1}{2} \|y_p - S_p C x\|^2 + \beta(x), \quad (2)$$

where \hat{x} is the reconstructed MR image using the algorithm, and $\beta(x)$ is the regularization term that is used to shrink the solution space. Traditionally, total variation using gradients in the image [4], \mathcal{L}_1 norm in the Wavelet domain [28] or \mathcal{L}_2 norm of the reconstruction [33] have been widely adopted as regularization terms. However, the classic approach for deep reconstruction models is to learn $\beta(x)$ during the offline training.

3.2 Structured State Space Models

Structured State Space Models (SSMs) are used for 1D sequence $x(t) \in \mathbb{R}$ to sequence $y(t) \in \mathbb{R}$ transformation using an implicit latent space $h(t) \in \mathbb{R}^N$ as follows

$$h'(t) = \mathbf{A}h(t) + \mathbf{B}x(t) \quad (3)$$

$$y(t) = \mathbf{C}h(t), \quad (4)$$

where $A \in \mathbb{R}^{N \times N}$, $B \in \mathbb{R}^{N \times 1}$ and $C \in \mathbb{R}^{1 \times N}$. Discretization is needed to integrate this continuous system to the existing deep learning frameworks. Discretization is generally performed via zero-order hold (ZOH) where Δ parameter comes into space to redefine continuous parameters A and B in the discrete form as follows

$$\bar{A} = \exp(\Delta A) \quad (5)$$

$$\bar{B} = (\Delta A)^{-1}(\exp(\Delta A) - I) \cdot \Delta B. \quad (6)$$

With this, we can rewrite the equations (3) and (4) as follows

$$h_t = \bar{A}h_{t-1} + \bar{B}x_t \quad (7)$$

$$y_t = Ch_t. \quad (8)$$

The selective scan mechanism proposed in Mamba makes the learnable parameters input dependent (dynamic) where $B \in \mathbb{R}^{Bs \times L \times N}$, $C \in \mathbb{R}^{Bs \times L \times N}$ and $\Delta \in \mathbb{R}^{Bs \times L \times D}$ are defined using linear projections of the input sequence $x \in \mathbb{R}^{Bs \times L \times D}$ where Bs corresponds to batch size, L to sequence length, D to number of channels in the input and N to inner state dimension.

4 Methodology

We adapt the Visual State Space Model (VSSM) blocks proposed in [26] for our physics-guided model, as shown in Figure 1. Following VSSM, we simply divide the input coil-combined complex MR images into patches with size p and perform unfolding in VSSM using 4 different directions (top-left to bottom-right, bottom-right to top-left,

top-right to bottom-left, and bottom-left to top-right) as shown in Figure 1. Unfolding in different directions is needed when employing SSMs in visual data, since the original SSMs are causal and span the input sequence in a single direction which is suitable for time-series data or language processing but contradicts the non-causal nature of images. We use L_1 norm of the difference between reconstructed and fully-sampled coil-combined images as the training objective, while employed AdamW optimizer is enforcing a decoupled weight decay [27] on the network weights. Our simplified training objective can be written as follows

$$\theta^* = \operatorname{argmin}_\theta \mathbb{E}_{(x_{us}, x_{fs}) \sim p_{\text{data}}} [\|x_{fs} - x_r(x_{us}, \mathcal{M}, C; \theta)\|_1] \quad (9)$$

where x_{us} and x_{fs} refers to the paired under- and fully-sampled coil-combined MR images, x_r refers to the reconstructed image, \mathcal{M} denotes the undersampling mask, C denotes the coil sensitivities, and θ refers to the model parameters.

To incorporate the complex MRI data, we convert complex MR images to real images using 2 separate channels for the real and imaginary components. In data-consistency blocks, we project patchified images back to the original shape with 2-channels via fully-connected layer, to convert them back to the complex form, and take centered Fourier transform. Then, we replace the generated k-space points with the acquired k-space points using the undersampling mask and the coil sensitivity maps, which are estimated using ESPIRiT [41] with default parameters, as shown in Eqs. (10) and (11). The steps sequentially followed in the i th data-consistency block can be expressed as

$$x_{dc}^i = \mathcal{F}^{-1}[\mathcal{F}[CU(x_p^i)] \odot (1 - \mathcal{M}) + \mathcal{F}[Cx_{us}] \odot \mathcal{M}] \quad (10)$$

$$x_{dc,p}^i = \mathcal{P}(\text{SiLU}(x_{dc}^i)) \quad (11)$$

where \mathcal{F} and \mathcal{F}^{-1} denotes forward and backward 2D Fourier Transforms, respectively, \mathcal{P} denotes the convolution-based patch embedding layer, \mathcal{U} represents the unpatchify layer, x_p^i is patchified input of the i th data-consistency layer, x_{dc}^i is redundant intermediate output, $x_{dc,p}^i$ is patchified output of the i th data-consistency layer, and SiLU is the swish [36] activation function.

In this design of architecture, we enable the information to be flown through patches in every possible directions, while keeping the reliance to the physical model by enforcing hard data-consistency between the VSSM blocks.

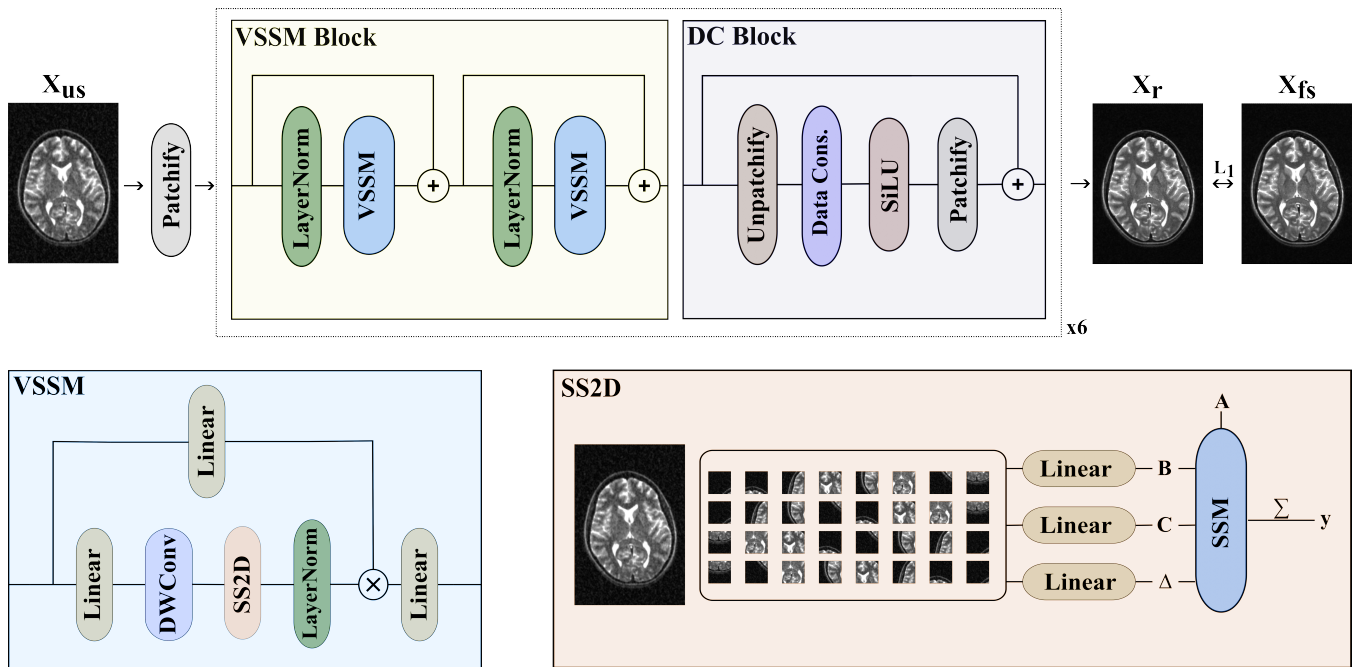


Figure 1: MambaRecon architecture is shown. X_{us} corresponds to zero-filled input image, X_{fs} is the fully sampled ground truth and X_r is the reconstructed image. Minimization of L_1 norm of the difference between X_{fs} and X_r is utilized as the training objective. Consecutive VSSM and data-consistency blocks (shown as DC Block) are repeated 6 times. Σ corresponds to summation across all unfolded vectors in the output of SSM. DWConv corresponds to the depth-wise convolution [17].

Table 1: Reconstruction metrics shown in the fastMRI dataset when $R = 4$ and 8.

| | T_1 -4x | | T_1 -8x | | T_2 -4x | | T_2 -8x | | Flair-4x | | Flair-8x | |
|-----------------|--------------|--------------|--------------|--------------|--------------|--------------|--------------|--------------|--------------|--------------|--------------|--------------|
| | | | | | PSNR (dB) | | SSIM (%) | | | | | |
| UNET | 30.93 | 86.55 | 27.94 | 80.97 | 28.65 | 83.82 | 26.23 | 78.07 | 28.09 | 83.75 | 25.32 | 76.70 |
| E2E-Varnet | 41.30 | 96.76 | 36.11 | 93.78 | 36.64 | 95.82 | 33.19 | 92.86 | 36.91 | 94.60 | 32.33 | 89.44 |
| RecurrentVarnet | 43.29 | 97.44 | 38.09 | 95.05 | 38.80 | 96.95 | 34.83 | 94.39 | 38.54 | 95.78 | 34.11 | 91.40 |
| SwinUNET | 35.89 | 93.53 | 33.04 | 91.06 | 32.42 | 91.95 | 30.28 | 88.99 | 31.93 | 90.31 | 29.16 | 85.90 |
| SwinMR | 38.42 | 94.03 | 35.28 | 91.57 | 33.90 | 92.74 | 31.22 | 89.65 | 34.20 | 91.15 | 31.09 | 86.39 |
| MambaRecon | 43.93 | 97.63 | 39.08 | 95.43 | 39.43 | 97.45 | 35.47 | 95.25 | 39.21 | 96.36 | 34.84 | 92.28 |

4.1 Network and Training Details

AdamW optimizer is used for training with default parameters for 100,000 iterations with a batch size of 4. Learning rate is decayed after warm-up using half-cycle cosine decay starting from 1×10^{-3} to 1×10^{-6} . Patch size is selected as 2 although 1, 4 and 8 are considered during hyper-parameter tuning as shown in ablation studies. Number of consecutive VSSM and data-consistency blocks are selected as 6; 4 and 8 are also considered as shown in the ablation studies. Inner state dimension of VSSM is selected as 16 following [26], while hidden dimension of features is selected as 128. SiLU activation [8] is used as the non-linearity throughout the network.

5 Experiments

Each competing method is trained end-to-end using under and fully-sampled image pairs. Acceleration is performed via variable-density 2D Gaussian masks with variance adjusted to achieve 4 and 8 acceleration rates. All experiments are performed on a single NVIDIA RTX A5000 gpu with a PyTorch framework. Number of parameters for each model has been shown in Table 3.

5.1 Datasets

We used the following magnitude single-coil and complex multi-coil brain MRI datasets in our experiments.

1. **fastMRI**: Multi-coil brain MRI dataset [23] is considered, subjects are divided into training, validation and testing as (100, 10, 40). T_1 -, T_2 -weighted

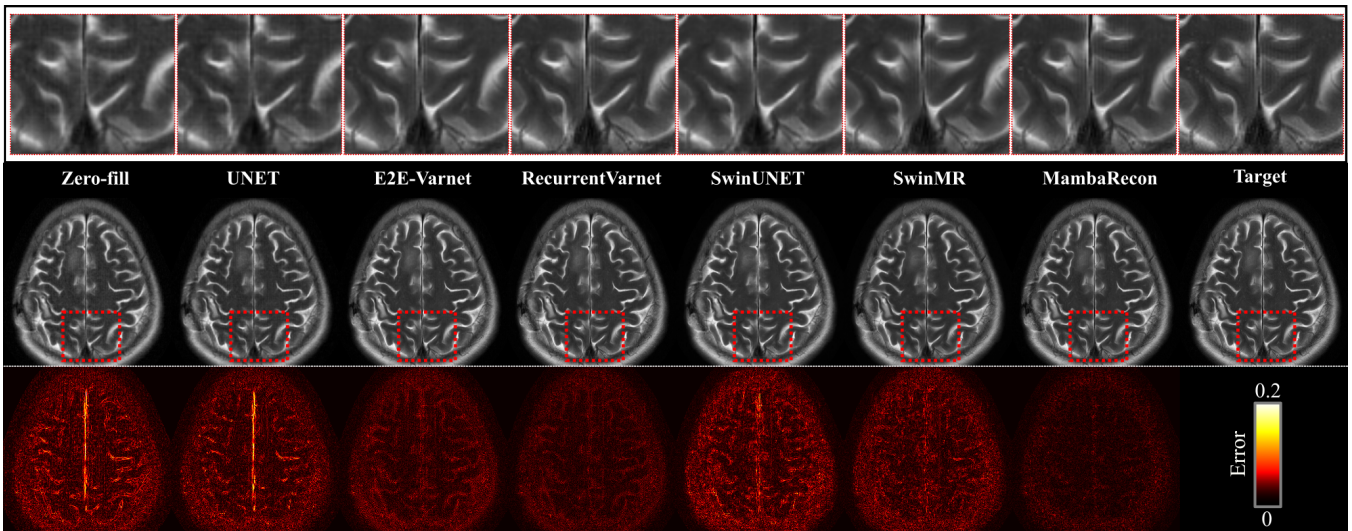


Figure 2: Reconstructions of T_2 images with acceleration rate of 4 from fastMRI. Zoomed-in areas and error maps are attached on top and below of reconstructions.

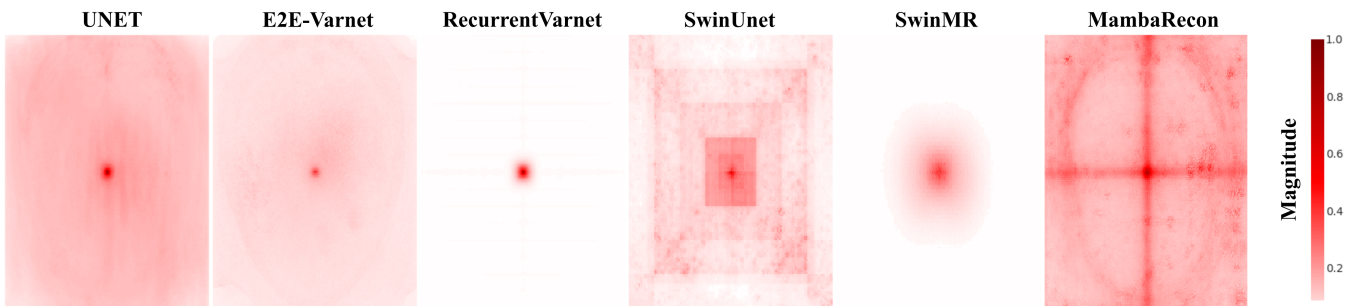


Figure 3: Effective receptive fields of each competing method are drawn after training, adapting the codes provided by [26]. Gradients are averaged across 100 test slices in fastMRI dataset. For physics-guided methods undersampling mask is given as zero to isolate the effect of the backbone. Each data point in these graphs represents the derivative of the center point in the reconstructed image with respect to the undersampled input image. A higher density of outer points indicates a stronger relationship between the center point and those locations, suggesting greater long-range sensitivity.

and Flair acquisitions are considered. There are no common protocol for all subjects. Number of coils are reduced to 5 to decrease the computational expense using [54]. Coil sensitivity maps are estimated using ESPIRiT with default parameters [41].

2. **IXI**: Single-coil brain MRI data from IXI (<http://brain-development.org/ixi-dataset/>) is considered. T_1 -, T_2 - and PD-weighted acquisitions are used. 25 subjects are used for training, 5 for validation and 10 for testing in all experiments.

5.2 Competing Methods

- **UNET**: U-shaped network model is utilized from [23]. Network hyper-parameters and implementation codes are gathered from [50]. Adam optimizer

is used with the default parameters with a learning rate of 0.002, for 150,000 number of iterations.

- **E2E-Varnet**: End-to-end variational network is considered [40]. Network hyper-parameters and implementation codes are gathered from [50]. Adam optimizer is used with the default parameters with a learning rate of 0.0002, for 150,000 iterations.
- **RecurrentVarnet**: An unrolled k-space based recurrent variational model is considered [51]. Network hyper-parameters and implementation codes are gathered from [50]. Adam optimizer is used with the default parameters with a learning rate of 0.0005, for 500,000 iterations.
- **SwinUnet**: A transformer based U-shaped segmentation model is adapted for MRI reconstruction

Table 2: Reconstruction metrics shown in the IXI dataset when $R = 4$ and 8.

| | T ₁ -4x | | T ₁ -8x | | T ₂ -4x | | T ₂ -8x | | PD-4x | | PD-8x | |
|-----------------|----------------------|--------------|--------------------|--------------|--------------------|--------------|--------------------|--------------|--------------|--------------|--------------|--------------|
| | PSNR (dB) SSIM (%) | | | | | | | | | | | |
| UNET | 37.01 | 94.07 | 31.82 | 90.57 | 38.06 | 94.85 | 33.86 | 91.98 | 36.99 | 94.66 | 32.04 | 91.43 |
| E2E-Varnet | 41.94 | 98.56 | 35.72 | 97.21 | 42.96 | 98.69 | 37.23 | 97.34 | 42.63 | 98.83 | 35.23 | 97.59 |
| RecurrentVarnet | 44.95 | 99.48 | 37.78 | 98.55 | 46.24 | 99.25 | 39.62 | 98.32 | 45.96 | 99.34 | 37.96 | 98.45 |
| SwinUNET | 34.77 | 94.73 | 30.59 | 91.75 | 37.54 | 95.11 | 33.92 | 92.44 | 32.58 | 94.71 | 29.32 | 91.59 |
| SwinMR | 38.30 | 96.05 | 33.76 | 93.65 | 40.03 | 96.17 | 35.75 | 93.89 | 38.34 | 96.14 | 33.66 | 93.61 |
| MambaRecon | 45.59 | 98.52 | 38.93 | 98.75 | 46.95 | 98.07 | 40.75 | 98.49 | 46.81 | 98.28 | 39.55 | 98.63 |

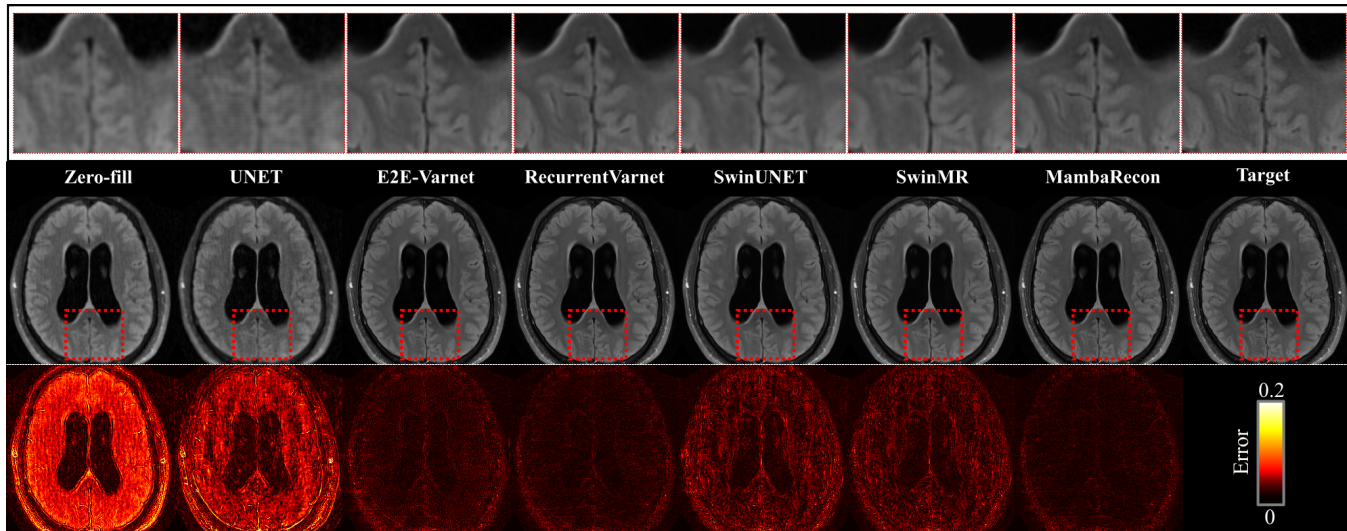


Figure 4: Reconstructions of Flair images with acceleration rate of 8 from fastMRI. Zoomed-in areas and error maps are attached on top and below of reconstructions.

Table 3: The number of parameters for each competing model is presented, with MambaRecon having the fewest parameters.

| Method | #Parameters |
|-----------------|-------------|
| UNET | 7.76e+6 |
| E2E-Varnet | 1.16e+7 |
| RecurrentVarnet | 2.83e+6 |
| SwinUNET | 2.71e+7 |
| SwinMR | 5.84e+6 |
| MambaRecon | 2.05e+6 |

[5]. AdamW optimizer is utilized for training with a learning rate of 0.0002 decayed after 5th epoch using cosine decay. Training is lasted for 100,000 iterations.

- **SwinMR**: A swin-transformer based MRI reconstruction model is considered [19]. Adam optimizer is used with the default parameters with a learning rate of 0.0002, for 100,000 iterations.

5.3 Ablation Studies

We perform a variety of ablation studies to show the individual effect of hyper-parameters and design choices. Performance metrics for ablation experiments are shown in Table 4. As the metrics indicate, using an overly deep model or a very small patch size led to performance loss in addition to an increased computational budget. Here we list the ablation studies performed:

1. OnlyDC: MambaRecon with only data-consistency blocks are considered where we removed the VSSM blocks completely from the model.
2. SwinRecon: MambaRecon with swin transformer blocks is considered where we replaced VSSM blocks with swin transformer blocks with the same hidden dimension (128) and patch size ($p = 2$). Window size is specified as 8.
3. MambaRecon with more shallow and deeper backbones is considered with depth = 4 and 8 respectively. Here depth represents number of consecutive VSSM and data-consistency block pairs.
4. MambaRecon with different patch sizes is consid-

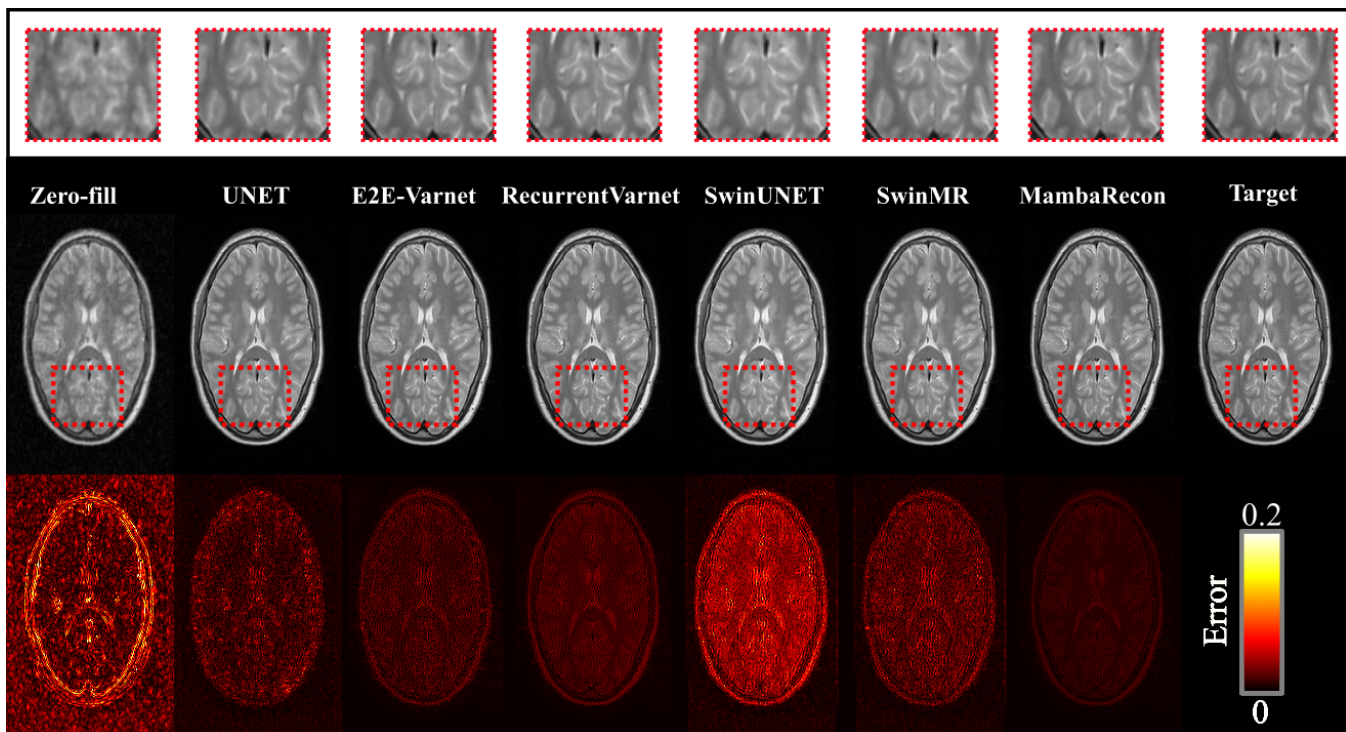


Figure 5: Reconstructions of PD images with acceleration rate of 4 from IXI. Zoomed-in areas and error maps are attached on top and below of reconstructions.

Table 4: Ablation results shown in fastMRI dataset when $R = 4$ and 8.

| | T ₁ -4x | | T ₁ -8x | | T ₂ -4x | | T ₂ -8x | | FLAIR-4x | | FLAIR-8x | |
|------------------|--------------------|--------------|--------------------|--------------|--------------------|--------------|--------------------|--------------|--------------|--------------|--------------|--------------|
| | PSNR (dB) | | | | SSIM (%) | | | | | | | |
| OnlyDC | 39.10 | 96.25 | 34.53 | 92.93 | 34.65 | 94.49 | 31.52 | 90.94 | 35.44 | 94.13 | 30.95 | 88.73 |
| SwinRecon | 43.53 | 97.68 | 38.40 | 95.30 | 38.94 | 97.19 | 34.86 | 94.81 | 38.79 | 96.19 | 34.34 | 91.89 |
| <i>Depth</i> = 4 | 43.59 | 97.66 | 38.74 | 95.36 | 39.25 | 97.32 | 35.18 | 94.99 | 38.85 | 96.13 | 34.55 | 91.90 |
| <i>Depth</i> = 8 | 43.61 | 97.74 | 39.00 | 95.49 | 39.10 | 97.33 | 35.29 | 95.12 | 38.91 | 96.25 | 34.57 | 92.19 |
| <i>p</i> = 1 | 43.67 | 97.80 | 38.59 | 95.21 | 39.12 | 97.28 | 34.92 | 94.68 | 38.95 | 96.36 | 34.38 | 91.71 |
| <i>p</i> = 4 | 42.51 | 97.24 | 37.81 | 94.74 | 38.07 | 96.68 | 34.55 | 94.32 | 37.96 | 95.56 | 33.90 | 91.27 |
| <i>p</i> = 8 | 39.83 | 96.22 | 36.39 | 93.86 | 35.61 | 95.15 | 33.29 | 92.96 | 35.80 | 93.78 | 32.73 | 89.81 |
| MambaRecon | 43.93 | 97.63 | 39.08 | 95.43 | 39.43 | 97.45 | 35.47 | 95.25 | 39.21 | 96.36 | 34.84 | 92.28 |

ered where p ranged from 1 to 8.

6 Results

We conducted a comprehensive comparison of MambaRecon against a diverse range of models and datasets to thoroughly evaluate its performance. Our benchmark included state-of-the-art physics-guided CNN-based models, E2E-Varnet and RecurrentVarnet, which leverage physical model for enhanced image reconstruction. We also included transformer-based reconstruction baselines, represented by SwinUNET and SwinMR, that utilize advanced transformer architectures to capture long range dependencies. Lastly, we considered a pure data-driven CNN-based network, exemplified by

UNET, which relies solely on data for image reconstruction. We considered both multi-coil complex and single-coil magnitude MRI datasets represented by fastMRI and IXI respectively. This diverse selection allowed us to assess our model’s capabilities across various reconstruction paradigms, from physics-guided approaches to advanced transformer-based and traditional CNN-based methods.

Peak Signal to Noise Ratio (PSNR) and Structural Similarity Index Measure (SSIM) [43] are considered as the comparison metrics. Results are presented separately for each acceleration rate and contrast pair. Best results are highlighted as bold for each test case. Table 1 and Table 2 present the performance metrics for fastMRI and IXI respectively. Figure 2 shows representative re-

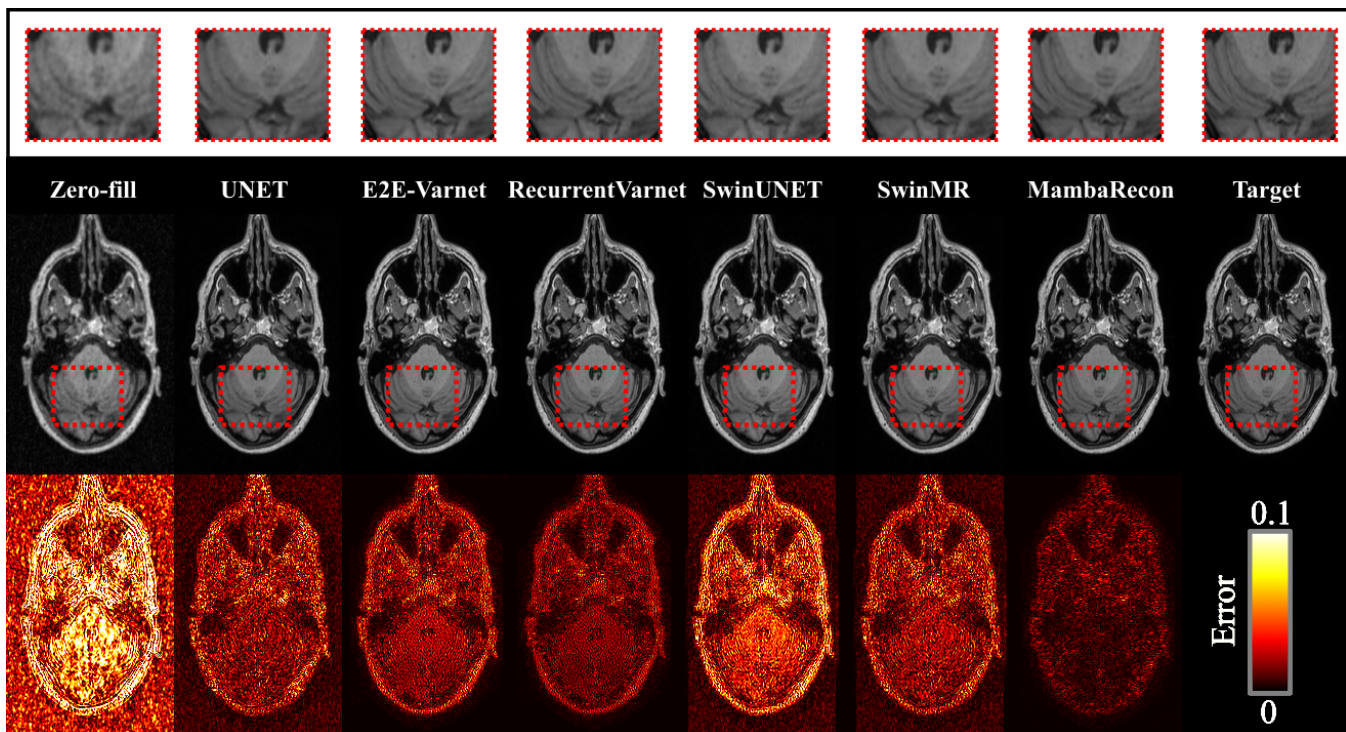


Figure 6: Reconstructions of T_1 -weighted images with acceleration rate of 4 from IXI. Zoomed-in areas and error maps are attached on top and below of reconstructions.

constructions of a T_2 -weighted slice with an acceleration rate of 4, Figure 4 stands for a Flair weighted slice when acceleration rate of 8 from fastMRI dataset. Figure 5 and Figure 6 stand for PD and T_1 -weighted reconstructions when acceleration rate of 4 from IXI dataset.

Quantitatively, compared with the second best method; MambaRecon yields 0.72dB more average PSNR in the fastMRI dataset and 1.01dB more average PSNR in the IXI dataset. Visually, MambaRecon captured almost all of the high frequency details hence yields the darkest error maps in the reconstruction figures without suffering from over-smoothing effect or noise. We also illustrate the effective receptive field of each competing method in Figure 3. We observe the most powerful receptive field corresponds to MambaRecon which yields a global receptive field spanning the whole image. We present the number of parameters in each competing method in Table 3.

7 Discussion and Future Work

We proposed a lightweight and efficient reconstruction model combining SSMS with physics-guided MRI models. To overcome the limitations of the original SSMS’ single-direction spanning, we adopted a multi-directional spanning approach. However, this approach might be less optimal than self-attention transformers in fully capturing the interactions between image patches. Implementing

a more advanced scanning technique could enhance the model’s performance.

Our method currently relies on ESPIRiT [41] for coil sensitivity estimation. By integrating this process within a unified framework, we could enable end-to-end training, potentially enhancing the efficiency and accuracy of the overall model. This unified approach would streamline the workflow, allowing for simultaneous optimization of both the coil sensitivity estimation and the subsequent image reconstruction, thereby improving performance.

Our model, like all other competing methods, is trained in a supervised manner using under-sampled and fully-sampled images from public MRI datasets. To eliminate the dependency on supervised training, a self-supervised training loss, as demonstrated by [46], could be employed. Moreover, a test-time adaptation approach could be beneficial to incorporate the changes in physical-model like acceleration rate or under-sampling pattern. We leave this exploration for future work.

8 Conclusion

We proposed a physics-guided MRI reconstruction framework utilizing structured state space models in its core. Our model benefits from high long range contextual sensitivity without creating a computational burden and yields a better reconstruction quality compared with the state-of-the-art reconstruction baselines.

References

- [1] H. K. Aggarwal, M. P. Mani, and M. Jacob. MoDL: Model-Based deep learning architecture for inverse problems. *IEEE Transactions on Medical Imaging*, 38(2):394–405, 2019. [1](#), [2](#)
- [2] Omer F Atli, Bilal Kabas, Fuat Arslan, Mahmut Yurt, Onat Dalmaz, and Tolga Çukur. I2i-mamba: Multimodal medical image synthesis via selective state space modeling. *arXiv preprint arXiv:2405.14022*, 2024. [2](#)
- [3] Sampurna Biswas, Hemant K Aggarwal, and Mathews Jacob. Dynamic MRI using model-based deep learning and SToRM priors: MoDL-SToRM. *Magnetic resonance in medicine*, 82(1):485–494, 2019. [2](#)
- [4] Kai Tobias Block, Martin Uecker, and Jens Frahm. Undersampled radial mri with multiple coils. iterative image reconstruction using a total variation constraint. *Magnetic Resonance in Medicine: An Official Journal of the International Society for Magnetic Resonance in Medicine*, 57(6):1086–1098, 2007. [3](#)
- [5] Hu Cao, Yueyue Wang, Joy Chen, Dongsheng Jiang, Xiaopeng Zhang, Qi Tian, and Manning Wang. Swin-unet: Unet-like pure transformer for medical image segmentation. In *European conference on computer vision*, pages 205–218. Springer, 2022. [6](#)
- [6] Salman UH Dar, Mahmut Yurt, Mohammad Shahdloo, Muhammed Emrullah Ildız, Berk Tinaz, and Tolga Çukur. Prior-guided image reconstruction for accelerated multi-contrast MRI via generative adversarial networks. *IEEE Journal of Selected Topics in Signal Processing*, 14(6):1072–1087, 2020. [1](#), [2](#)
- [7] David L Donoho, Arian Maleki, and Andrea Montanari. Message-passing algorithms for compressed sensing. *Proceedings of the National Academy of Sciences*, 106(45):18914–18919, 2009. [1](#)
- [8] Stefan Elfving, Eiji Uchibe, and Kenji Doya. Sigmoid-weighted linear units for neural network function approximation in reinforcement learning. *Neural networks*, 107:3–11, 2018. [4](#)
- [9] Taejoon Eo, Yohan Jun, Taeseong Kim, Jinseong Jang, Ho-Joon Lee, and Dosik Hwang. Kiki-net: cross-domain convolutional neural networks for reconstructing undersampled magnetic resonance images. *Magnetic resonance in medicine*, 80(5):2188–2201, 2018. [2](#)
- [10] Zalan Fabian, Berk Tinaz, and Mahdi Soltanolkotabi. Humus-net: Hybrid unrolled multi-scale network architecture for accelerated mri reconstruction. *Advances in Neural Information Processing Systems*, 35:25306–25319, 2022. [2](#)
- [11] Albert Gu and Tri Dao. Mamba: Linear-time sequence modeling with selective state spaces. *arXiv preprint arXiv:2312.00752*, 2023. [1](#)
- [12] Albert Gu, Karan Goel, and Christopher Ré. Efficiently modeling long sequences with structured state spaces. *arXiv preprint arXiv:2111.00396*, 2021. [1](#)
- [13] Alper Güngör, Salman UH Dar, Şaban Öztürk, Yilmaz Korkmaz, Hasan A Bedel, Gokberk Elmas, Muzaffer Ozbey, and Tolga Çukur. Adaptive diffusion priors for accelerated mri reconstruction. *Medical image analysis*, 88:102872, 2023. [2](#)
- [14] Hang Guo, Jinmin Li, Tao Dai, Zhihao Ouyang, Xudong Ren, and Shu-Tao Xia. Mambair: A simple baseline for image restoration with state-space model. *arXiv preprint arXiv:2402.15648*, 2024. [1](#)
- [15] Pengfei Guo, Yiqun Mei, Jinyuan Zhou, Shanshan Jiang, and Vishal M Patel. Reconformer: Accelerated mri reconstruction using recurrent transformer. *IEEE transactions on medical imaging*, 2023. [1](#), [2](#)
- [16] Justin P Haldar, Diego Hernando, and Zhi-Pei Liang. Compressed-sensing mri with random encoding. *IEEE transactions on Medical Imaging*, 30(4):893–903, 2010. [1](#)
- [17] Andrew G Howard, Menglong Zhu, Bo Chen, Dmitry Kalenichenko, Weijun Wang, Tobias Weyand, Marco Andreetto, and Hartwig Adam. Mobilenets: Efficient convolutional neural networks for mobile vision applications. *arXiv preprint arXiv:1704.04861*, 2017. [4](#)
- [18] Dianlin Hu, Yikun Zhang, Jianfeng Zhu, Qiegen Liu, and Yang Chen. Trans-net: Transformer-enhanced residual-error alternative suppression network for mri reconstruction. *IEEE Transactions on Instrumentation and Measurement*, 71:1–13, 2022. [2](#)
- [19] Jiahao Huang, Yingying Fang, Yinzhe Wu, Huanjun Wu, Zhifan Gao, Yang Li, Javier Del Ser, Jun Xia, and Guang Yang. Swin transformer for fast mri. *Neurocomputing*, 493:281–304, 2022. [1](#), [2](#), [6](#)
- [20] Jiahao Huang, Liutao Yang, Fanwen Wang, Yinzhe Wu, Yang Nan, Angelica I Aviles-Rivero, Carola-Bibiane Schönlieb, Daoqiang Zhang, and Guang Yang. Mambamir: An arbitrary-masked mamba for joint medical image reconstruction and uncertainty estimation. *arXiv preprint arXiv:2402.18451*, 2024. [2](#)
- [21] Chang Min Hyun, Hwa Pyung Kim, Sung Min Lee, Sungchul Lee, and Jin Keun Seo. Deep learning for undersampled MRI reconstruction. *Physics in Medicine and Biology*, 63(13):135007, 2018. [2](#)
- [22] Feyza Duman Keles, Pruthuvi Mahesakya Wijewardena, and Chinmay Hegde. On the computational complexity of self-attention. In *International Conference on Algorithmic Learning Theory*, pages 597–619. PMLR, 2023. [1](#)
- [23] Florian Knoll, Jure Zbontar, Anuroop Sriram, Matthew J. Muckley, Mary Bruno, Aaron Defazio, Marc Parente, Krzysztof J. Geras, Joe Katsnelson, Hersh Chandarana, Zizhao Zhang, Michal Drozdal, Adriana Romero, Michael Rabbat, Pascal Vincent, James Pinkerton, Duo Wang, Nafissa Yakubova, Erich Owens, C. Lawrence Zitnick, Michael P. Recht, Daniel K. Sodickson, and Yvonne W. Lui. fastMRI: A publicly available raw k-space and DICOM dataset of knee images for accelerated MR image reconstruction using machine learning. *Radiology: Artificial Intelligence*, 2(1):e190007, 2020. [4](#), [5](#)
- [24] Yilmaz Korkmaz, Salman UH Dar, Mahmut Yurt, Muzaffer Özbey, and Tolga Çukur. Unsupervised mri reconstruction via zero-shot learned adversarial transformers. *IEEE Transactions on Medical Imaging*, 2022. [1](#), [2](#)
- [25] Dongwook Lee, Jaejun Yoo, Sungho Tak, and Jong Chul Ye. Deep residual learning for accelerated mri using

- magnitude and phase networks. *IEEE Transactions on Biomedical Engineering*, 65(9):1985–1995, 2018. 1, 2
- [26] Yue Liu, Yunjie Tian, Yuzhong Zhao, Hongtian Yu, Lingxi Xie, Yaowei Wang, Qixiang Ye, and Yunfan Liu. Vmamba: Visual state space model. *arXiv preprint arXiv:2401.10166*, 2024. 1, 3, 4, 5
- [27] Ilya Loshchilov and Frank Hutter. Decoupled weight decay regularization. *arXiv preprint arXiv:1711.05101*, 2017. 3
- [28] Michael Lustig, David Donoho, and John M Pauly. Sparse mri: The application of compressed sensing for rapid mr imaging. *Magnetic Resonance in Medicine: An Official Journal of the International Society for Magnetic Resonance in Medicine*, 58(6):1182–1195, 2007. 1, 3
- [29] Michael Lustig, David L Donoho, Juan M Santos, and John M Pauly. Compressed sensing mri. *IEEE signal processing magazine*, 25(2):72–82, 2008. 1
- [30] Jun Lyu, Guangyuan Li, Chengyan Wang, Chen Qin, Shuo Wang, Qi Dou, and Jing Qin. Region-focused multi-view transformer-based generative adversarial network for cardiac cine mri reconstruction. *Medical Image Analysis*, 85:102760, 2023. 2
- [31] Jun Ma, Feifei Li, and Bo Wang. U-mamba: Enhancing long-range dependency for biomedical image segmentation. *arXiv preprint arXiv:2401.04722*, 2024. 1
- [32] Ricardo Otazo, Daniel Kim, Leon Axel, and Daniel K Sodickson. Combination of compressed sensing and parallel imaging for highly accelerated first-pass cardiac perfusion mri. *Magnetic resonance in medicine*, 64(3):767–776, 2010. 1
- [33] Klaas P Pruessmann, Markus Weiger, Markus B Scheidegger, and Peter Boesiger. Sense: sensitivity encoding for fast mri. *Magnetic Resonance in Medicine: An Official Journal of the International Society for Magnetic Resonance in Medicine*, 42(5):952–962, 1999. 3
- [34] Chen Qin, Jo Schlemper, Jose Caballero, Anthony N Price, Joseph V Hajnal, and Daniel Rueckert. Convolutional recurrent neural networks for dynamic mr image reconstruction. *IEEE transactions on medical imaging*, 38(1):280–290, 2018. 1
- [35] C. Qin, J. Schlemper, J. Caballero, A. N. Price, J. V. Hajnal, and D. Rueckert. Convolutional recurrent neural networks for dynamic MR image reconstruction. *IEEE Transactions on Medical Imaging*, 38(1):280–290, 2019. 2
- [36] Prajit Ramachandran, Barret Zoph, and Quoc V Le. Searching for activation functions. *arXiv preprint arXiv:1710.05941*, 2017. 3
- [37] Jiacheng Ruan and Suncheng Xiang. Vm-unet: Vision mamba unet for medical image segmentation. *arXiv preprint arXiv:2402.02491*, 2024. 2
- [38] Jo Schlemper, Jose Caballero, Joseph V Hajnal, Anthony Price, and Daniel Rueckert. A deep cascade of convolutional neural networks for mr image reconstruction. In *Information Processing in Medical Imaging: 25th International Conference, IPMI 2017, Boone, NC, USA, June 25–30, 2017, Proceedings 25*, pages 647–658. Springer, 2017. 1, 2
- [39] Anuroop Sriram, Jure Zbontar, Tullie Murrell, Aaron Defazio, C. Lawrence Zitnick, Nafissa Yakubova, Florian Knoll, and Patricia Johnson. End-to-end variational networks for accelerated MRI reconstruction. In Anne L. Martel, Purang Abolmaesumi, Danail Stoyanov, Diana Mateus, Maria A. Zuluaga, S. Kevin Zhou, Daniel Racoceanu, and Leo Joskowicz, editors, *Proceedings of MICCAI*, pages 64–73, 2020. 2
- [40] Anuroop Sriram, Jure Zbontar, Tullie Murrell, Aaron Defazio, C Lawrence Zitnick, Nafissa Yakubova, Florian Knoll, and Patricia Johnson. End-to-end variational networks for accelerated mri reconstruction. In *Medical Image Computing and Computer Assisted Intervention—MICCAI 2020: 23rd International Conference, Lima, Peru, October 4–8, 2020, Proceedings, Part II 23*, pages 64–73. Springer, 2020. 5
- [41] Martin Uecker, Peng Lai, Mark J Murphy, Patrick Virtue, Michael Elad, John M Pauly, Shreyas S Vasanawala, and Michael Lustig. Espirit—an eigenvalue approach to autocalibrating parallel mri: where sense meets grappa. *Magnetic resonance in medicine*, 71(3):990–1001, 2014. 3, 5, 8
- [42] Shanshan Wang, Zhenghang Su, Leslie Ying, Xi Peng, Shun Zhu, Feng Liang, Dagan Feng, and Dong Liang. Accelerating magnetic resonance imaging via deep learning. In *IEEE 13th International Symposium on Biomedical Imaging (ISBI)*, pages 514–517, 2016. 1, 2
- [43] Zhou Wang, Alan C Bovik, Hamid R Sheikh, and Eero P Simoncelli. Image quality assessment: from error visibility to structural similarity. *IEEE transactions on image processing*, 13(4):600–612, 2004. 7
- [44] Ziyang Wang, Jian-Qing Zheng, Yichi Zhang, Ge Cui, and Lei Li. Mamba-unet: Unet-like pure visual mamba for medical image segmentation. *arXiv preprint arXiv:2402.05079*, 2024. 1, 2
- [45] Zhaohu Xing, Tian Ye, Yijun Yang, Guang Liu, and Lei Zhu. Segmamba: Long-range sequential modeling mamba for 3d medical image segmentation. *arXiv preprint arXiv:2401.13560*, 2024. 2
- [46] Burhaneddin Yaman, Seyed Amir Hossein Hosseini, Steen Moeller, Jutta Ellermann, Kâmil Uğurbil, and Mehmet Akçakaya. Self-supervised learning of physics-guided reconstruction neural networks without fully sampled reference data. *Magnetic resonance in medicine*, 84(6):3172–3191, 2020. 1, 2, 8
- [47] Yan Yang, Jian Sun, Huibin Li, and Zongben Xu. Admm-csnet: A deep learning approach for image compressive sensing. *IEEE transactions on pattern analysis and machine intelligence*, 42(3):521–538, 2018. 2
- [48] Yijun Yang, Zhaohu Xing, and Lei Zhu. Vivim: a video vision mamba for medical video object segmentation. *arXiv preprint arXiv:2401.14168*, 2024. 2
- [49] Jong Chul Ye, Yoseob Han, and Eunju Cha. Deep convolutional framelets: A general deep learning framework for inverse problems. *SIAM Journal on Imaging Sciences*, 11(2):991–1048, 2018. 1, 2
- [50] George Yiasemis, Nikita Moriakov, Dimitrios Karkalousos, Matthan Caan, and Jonas Teuwen. Direct: Deep image reconstruction toolkit, 2022. 5

- [51] George Yiasemis, Jan-Jakob Sonke, Clarisa Sánchez, and Jonas Teuwen. Recurrent variational network: a deep learning inverse problem solver applied to the task of accelerated mri reconstruction. In *Proceedings of the IEEE/CVF conference on computer vision and pattern recognition*, pages 732–741, 2022. 2, 5
- [52] Yubiao Yue and Zhenzhang Li. Medmamba: Vision mamba for medical image classification. *arXiv preprint arXiv:2403.03849*, 2024. 2
- [53] Han Zhang, Ian Goodfellow, Dimitris Metaxas, and Augustus Odena. Self-attention generative adversarial networks. In *Proceedings of the 36th International Conference on Machine Learning*, pages 7354–7363, 2019. 1
- [54] Tao Zhang, John M Pauly, Shreyas S Vasanaawala, and Michael Lustig. Coil compression for accelerated imaging with cartesian sampling. *Magnetic resonance in medicine*, 69(2):571–582, 2013. 5
- [55] Xiang Zhao, Tiejun Yang, Bingjie Li, and Xin Zhang. Swingan: A dual-domain swin transformer-based generative adversarial network for mri reconstruction. *Computers in Biology and Medicine*, 153:106513, 2023. 2
- [56] Bo Zhou, Neel Dey, Jo Schlemper, Seyed Sadegh Mohseni Salehi, Chi Liu, James S Duncan, and Michal Sofka. Dsformer: A dual-domain self-supervised transformer for accelerated multi-contrast mri reconstruction. In *Proceedings of the IEEE/CVF winter conference on applications of computer vision*, pages 4966–4975, 2023. 2
- [57] Bo Zhou, Jo Schlemper, Neel Dey, Seyed Sadegh Mohseni Salehi, Chi Liu, James S Duncan, and Michal Sofka. Dsformer: A dual-domain self-supervised transformer for accelerated multi-contrast mri reconstruction. *arXiv preprint arXiv:2201.10776*, 2022. 1
- [58] Jing Zou, Lanqing Liu, Qi Chen, Shujun Wang, Xiaohan Xing, and Jing Qin. Mmr-mamba: Multi-contrast mri reconstruction with mamba and spatial-frequency information fusion. *arXiv preprint arXiv:2406.18950*, 2024. 2